INTEGRATING POTENTIAL FLOW CODE FOR SHIP BANK INTERACTION AT REAL TIME SIMULATIONS

Ibarrondo, Marta, MARIN, The Netherlands

Gornicz, Tomasz, MARIN, The Netherlands

Kleermaker, Wim, MARIN, The Netherlands

INTEGRATING POTENTIAL FLOW CODE FOR SHIP BANK INTERACTION AT REAL TIME SIMULATIONS

IBARRONDO, MARTA, MARIN, THE NETHERLANDS
GORNICZ, TOMASZ, MARIN, THE NETHERLANDS
KLEERMAKER, WIM, MARIN, THE NETHERLANDS

SUMMARY

The MARIN simulator utilizes an advanced method that runs on graphics processing units (GPUs) to estimate the hydrodynamic loads that occur when a ship navigates near a bank. This method is based on potential flow theory, which is particularly useful for modeling fluid flow around ships in various maritime conditions. Series of model tests, Computational Fluid Dynamics simulations, RAPID calculations and Extensible Modelling Framework (XMF) simulations using the Flow Interaction node were conducted using a 135-meter inland ship, which was equipped with two ducted propellers and four Schilling-type rudders. This study investigated the impact of key parameters—such as sailing speed, water depth, and proximity to the bank—on suction/repulsion forces. The results were analyzed with the initial aim of assessing the feasibility of the Flow Interaction code for practical applications at real time simulator. At this stage, the research focuses on understanding and refining the code's behavior in shallow water.

NOMENCLATURE

δ	Rudder angle (deg)
∇	Displacement volume (m^3)
λ	Linear scale ratio (-)
ρ	Fresh-water density (999,1 kg/m^3)
θ	Pitch angle (deg)
A_C	Cross-sectional area of the waterway (m^2)
A_S	Ship's underwater midship cross-sectional area (m^2)
B	Ship breadth (m)
C_P	Dynamic pressure coefficient (-)
d	Distance between the ship side and the bank (m)
d/B	Non-dimensional distance to bank (-)
F_r	Froude number (-)
F_{rh}	Depth Froude number (-)
$F'_{X\ or}\ C_x$	Ship surge force coefficient (-)
$F'_{Y\ or}\ C_y$	Ship sway force coefficient (-)
h	Water depth (m)
h/T	Water depth-to-draught ratio (-)
L_{PP}	Ship length between perpendiculars (m)
$M'_{Z\ or}\ C_z$	Ship yaw moment coefficient (-)
P/D	Pitch ratio at 70% radius (-)
RPM	Propeller revolution rate (1/min)
S	Blockage factor A_S/A_C (-)
T	Ship draught at rest (m)
V_{cr}	Critical canal speed (km/h or m/s)
V_s	Ship speed (km/h or m/s)
Z	Number of blades (-)
XMF	Extensible Modelling Framework
CPU	Central Processing Unit
GPU	Graphics Processing Unit
CFD	Computational Fluid Dynamics
RAPID	Raised Panel Iterative Dawson
RAPID NO TRIM	Raised Panel Iterative Dawson taking out trim and sinkage
BASIN	Experimental model test results
MARIN	Maritime Research Institute Netherlands
DST	Development Centre for Ship Technology and Transport Systems
SHINING	Shallow Water Inland Ships Manoeuvring working group
BAW	German Federal Waterways Engineering and Research Institute

1 INTRODUCTION

As ships grow in size and navigate more confined waterways, understanding ship-bank interactions has become crucial. Research focuses on predicting resistance, squat, and hydrodynamic forces near banks, with reduced-order models for suction and repulsion forces (Norrbin, 1985; Delefortrie et al., 2024) integrated into ship-handling simulators for training, waterway design, and accident analysis. Recent studies emphasize real-time predictions for safe navigation, including irregular banks (Bedos et al., 2019), shallow water maneuvering (Mai et al., 2021), and canal accessibility (Verwilligen et al., 2022). Model tests are resource-intensive, but advances in CFD provide a cost-effective alternative, although benchmarking remains critical. Van Hoydonck et al. (2019) highlight the importance of validating CFD methods, particularly for inland waterways with fluctuating water levels and narrow corridors. To overcome the limitations of traditional methods, the MARIN simulator uses advanced time domain computations and GPU power to improve hydrodynamic load estimations' in real time simulations.

The MARIN simulator's methodology is grounded in potential flow theory, a well-established approach for modeling fluid flow around ships. This theory offers a computationally efficient means of estimating the forces acting on a vessel without the heavy resource demands of full-scale CFD simulations. By leveraging GPU acceleration, the simulator enables faster and more efficient real-time predictions, making it an invaluable tool for ship designers, operators, and researchers aiming to enhance vessel performance in complex maritime environments. In this paper, the potential code will be referred to as the Flow Interaction Code within the XMF simulation package.

An extensive study was undertaken using a 135-meter inland vessel equipped with two ducted propellers and four Schilling-type rudders. This study integrated physical model tests (Bedos et al. 2025), high-fidelity CFD simulations, RAPID potential flow code based on a raised-panel method (Raven, 1995, 1996 and 1998) and Flow Interaction code in XMF (GPU-based) computations to rigorously assess the accuracy of the MARIN simulator's ship-bank interaction models. By comparing Flow Interaction generated results with CFD simulations and RAPID output, it is possible to evaluate the distribution of hydrodynamic loads along the ship's hull and identify key areas where the XMF based approach could be further refined.

This work explores how key parameters—such as sailing speed, water depth, and distance to the bank—affect suction forces. The results are compared with the ultimate goal of trying to make a first attempt to confirm the usability of the Flow interaction code for practical applications at real time simulator. At this stage the research is centred entirely on understanding behaviour of the code and improve its behaviour in shallow water rather than correction methods for including the viscous effects.

2 FLOW INTERACTION CODE

The flow interaction code was developed as the successor to PASSCAL and based on the work of Korsmeyer et al. 1993, was initially introduced as a CPU-based tool in 2017. However, it lacked the necessary computational speed and validation. In 2021, a GPU version was released, significantly improving speed but still facing robustness challenges. By 2023, the initiative was launched to validate the enhanced GPU code, which had become more stable but still required further refinements.

The Flow Interaction code assumes an idealized potential flow by neglecting viscosity, free-surface effects, and simplifying cross-flow vorticity using thin-wing theory. Various geometric simplifications are made based on the specific problem. For conventional ships at low Froude numbers, the assumptions about viscosity and free-surface effects are considered reasonable, as viscosity has minimal impact except in cases of cross-flow vorticity, and waves generated by ship motion are generally insignificant. However, the treatment of cross-flow vorticity is more uncertain and depends on the particular case.

Cross-flow drag along a ship's hull plays a crucial role in large-amplitude maneuvers, and similar effects may apply to ship interactions if transverse flow velocities are significant. In such cases, these effects can be idealized using a trailing vortex sheet downstream of the stern, with a Kutta condition applied by analogy to low-aspect-ratio wing theory. While this approach, as outlined by Newman. 1977, provides qualitative insights into maneuvering behavior, experimental comparisons show that it lacks quantitative accuracy due to the complexity of stern flow and interactions with propellers. Traditional slender-body theories approximate ship interactions based on their relative distances, but these methods only provide qualitative accuracy. To improve precision, the Flow Interaction code employs a numerical approach using three-dimensional panel methods, avoiding previous geometric assumptions.

The method computes interaction forces based on the panel method pioneered by Hess & Smith (1964), this is the first known application to ship interactions. By neglecting free-surface effects and shed vorticity, memory effects are removed, allowing time-stepped hydrodynamic calculations. The process involves deriving an integral equation for velocity potential, discretizing it using quadrilateral panels, solving the resulting algebraic system, and computing force and moment histories for each ship.

3 TEST CASES

The study focuses on a 135m CEMT-class Vb inland ship, commonly operating on the Rhine. Designed in 2014 by BAW and DST, this benchmark vessel has been used in experimental studies on resistance, propulsion, and maneuvering in shallow water (Mucha et al., 2017, 2018, 2019). More recently, it was selected in the SHINING workshop to evaluate CFD techniques for predicting maneuvering forces and moments in shallow water (Chilcee et al., 2025).

Table 1 details the inland waterway ship's main particulars and appendages at full scale and a linear scale ratio of 1:16. Experimental and CFD were conducted at model scale, while RAPID and Flow Interaction simulations were run full scale. The ship features a twin-shaft arrangement with two ducted propellers (1.6 m diameter, inward rotation) and four fishtail-type rudders with endplates. The duct geometry resembles the 19A type but is horizontally trimmed at the baseline. The rudders' projected lateral area is approximately 4 x 2.36 m^2 times, equating to 4 x 0.50%·L_{PP}·T. Further aft-ship details are provided by Mucha et al. 2017.

Table 1. Main particulars of the inland waterway ship and its appendages.

Designation	Symbol	Full scale	Model scale
Linear scale ratio (-)	λ	1	16
Length between perpendiculars (m)	L_{PP}	135.0	8.438
Breadth moulded on waterline (m)	B	11.44	0.715
Draught at rest, even keel (m)	T	3.50	0.219
Displacement volume (m^3)	∇	4,991.5	1.219
Propeller diameter (m)	B	1.6	0.100
Pitch ratio at 70% radius (-)	P/D	1.000	1.000
Expanded blade area ratio (-)	A_E/A_0	0.679	0.679
Number of blades (-)	Z	4	4
Rudder height (m)	b	1.726	0.108
Rudder chord (m)	c	1.370	0.086

This work compares experimental and numerical methods to analyse ship-bank interactions for a reference ship in shallow water, ensuring a fair comparison with a consistent setup. The ship sails along a vertical wall on its port side, with a parallel wall farther on the starboard side. The distance between them is 22.1 times the ship's width. The distance towards the closest bank varies between 2.0 to 1.0 B, therefore the system can be considered confined. The ship is towed in a semi-captive condition, with imposed surge, sway, roll, and yaw motions, while heave and pitch remain free, ensuring realistic force equilibrium. The study examines various portside bank distances (d/B) and water depths (h/T). The ship moves straight at a constant speed with fixed propeller RPM and neutral rudders. Dynamic squat, highly sensitive to hydrodynamic loads in shallow waters, is considered. Tests were conducted at 0.972 m/s (14 km/h full scale, Fr = 0.107) with a 4.5% blockage factor.

The tests used the ship model under two propeller regimes: self-propulsion and water milling, the latter aiding CFD comparisons. Experiments were conducted at three water depths (3.0, 1.5, and 1.2 h/T) to study deep and shallow water effects. Four bank distances (2.5, 2.0, 1.5, and 1.0 d/B) and four speeds (8, 10, 12, and 14 km/h) were tested to simulate real-life conditions and improve result reliability. Details on the setup of both the model tests and CFD calculations are provided in Bedos et al. (2025).

An overview of the runs carried out is presented in Table 2.

Table 2. Matrix of stationary conditions (quantities are indicated at model scale)

Run	h/T (-)	Vs (m/s)	d/B (-)	RPM (1/min)	δ (deg)	FI (-)	CFD (-)	RAPID (-)	RAPID NO TRIM (-)
02010401	3.0	0.972	1.5	303	0	✓	✓	✓	✓
03010201	1.5	0.972	2.0	322	0	✓	✓	✓	✓
03010301	1.5	0.972	1.5	322	0	✓	✓	✓	✓
03010401	1.5	0.972	1.0	322	0	✓	✓	✓	✓
04010301	1.2	0.972	1.5	341	0	✓	✓	✓	

4 RAPID/ FLOW INTERACTION CODE SETUPS

In order to perform the assessment, potential flow simulations were conducted using the XMF simulation package with the GPU[1] implementation.

As expected both in RAPID and Flow interaction code in XMF, elements such as ducts, rudders, and other intricate details can be omitted, as they are not incorporated into the simulation framework. The banks are represented as simplified flat vertical walls positioned on both sides of the vessel. Both numerical setups were done using full scale values. For sailing with the heading parallel to the bank only the u-velocity is set, for sailing with a 0 drift angle the u- and v-velocity are set such that the speed vector is pointing parallel to the bank. Table 3 summarises the main particulars of the numerical domains. Figure 1 and Figure 2 show a 3D view of the domain in both numerical tools.

Table 3. Numerical domain in Flow Interaction code and RAPID

Parameter name	FI	RAPID
Computational domain size (m)	2840	413.5 x 157.8
Vessel Grid Number of panels (-)	2246	7198
Port Bank Grid. Number of panels (-)	800	2370
Starboard Bank Grid. Number of panels (-)	800	2370

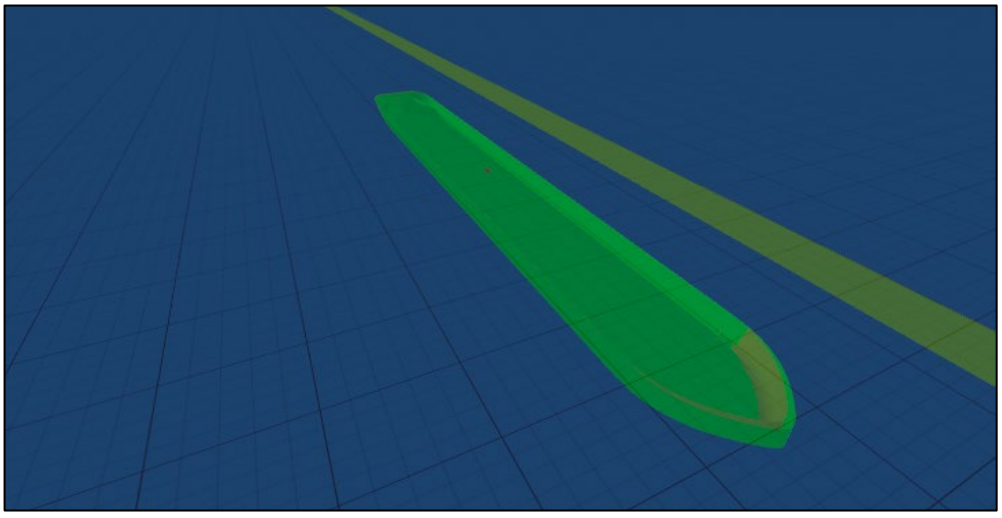

Figure 1. Computational domain in Flow Interaction

[1] The Parallel Flow Interaction between ships was verified against Flow Interaction via the test scripts used in the 2017 XMF-PASSCAL-Ropes comparison. These 35 scripts specified container-container and tanker-tanker interaction. Forces and moments showed a good resemblance but in some cases there were small differences due to calculation inaccuracies. GPU's floating point calculation is performed in single precision instead of double precision on a CPU.

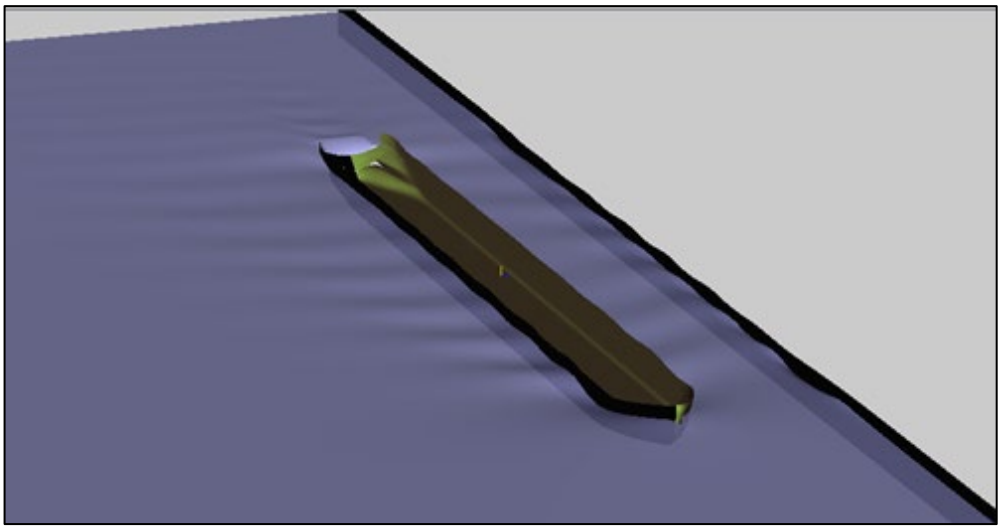

Figure 2. Computational domain in RAPID

To assess the influence of grid resolution on computational accuracy, five vessel grids were employed, ensuring that the aspect ratio and relative panel sizes remained consistent across refinements. The grid specifications are detailed in Table 4. Figure 3 presents a comparative analysis of the first, third, and fifth grid resolutions, highlighting the impact of grid refinement on the computational results.

Table 4. Flow Interaction set up. Hull grid number associated with number of panels.

Grid number	Panels
1	386
2	958
3	2246
4	3832
5	6138

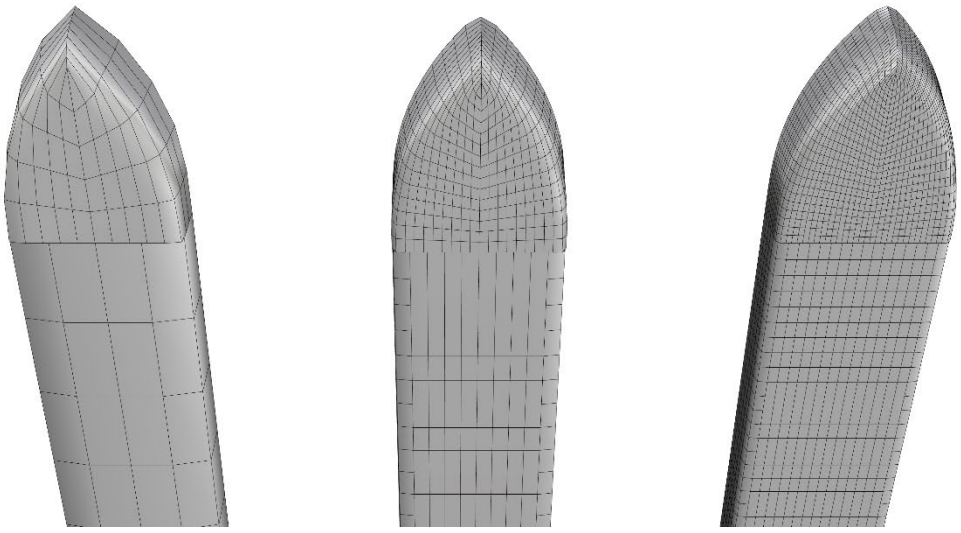

Figure 3. Hull grid 1 (left), 3 (centre) and 5 (right)

Figure 4 shows a longitudinal distribution of the side force Fy and yawing moment Mz. The plot is obtained by splitting the hull into a series of slices (sections) with a constant width. For every slice, the forces and moments are calculated. Then, the values are summed in the flow direction from the bow (x/Lpp=1) towards the transom (x/Lpp=0). The plot illustrates a build-up of Fy and Mz along the ship, starting with value zero at the bow and total force and moment acting on the ship given at x/Lpp=0.

For a single time step, the results across different grid resolutions are analyzed based on the integrated load distribution along the hull. Notably, the first two grids exhibit significant deviations, particularly in the moment calculations, compared to the finer grids. From grid 3 onward, the variation in results decreases, indicating improved numerical stability. Consequently, grid 3 is selected for all subsequent simulations in this study.

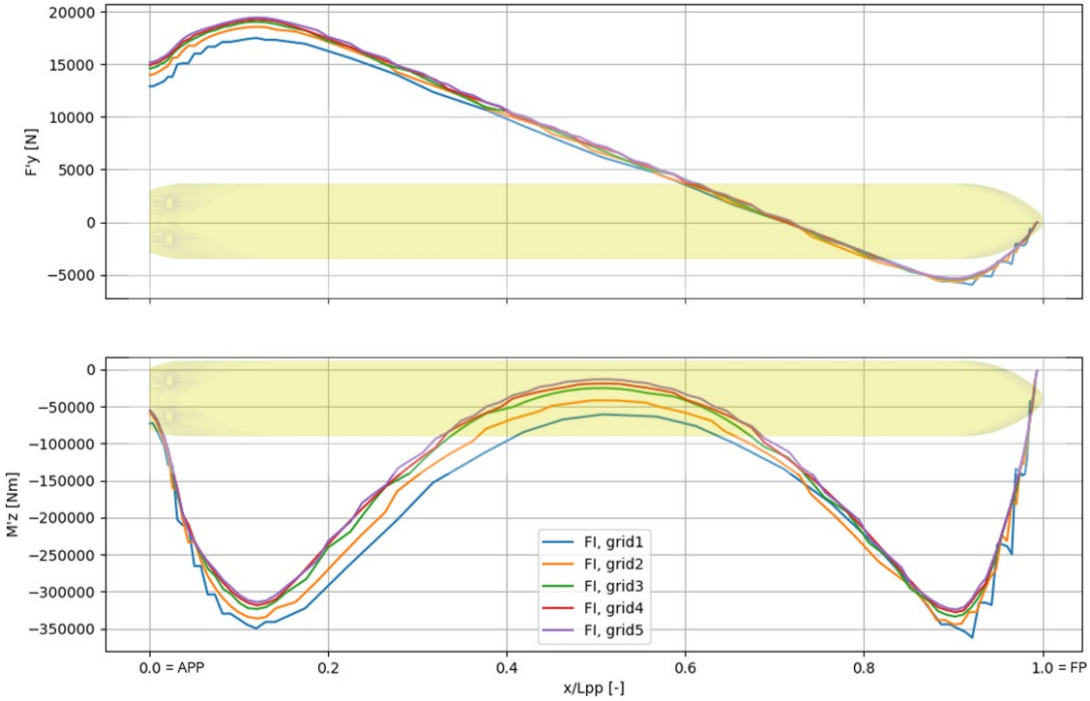

Figure 4. Comparison of longitudinal side force (Fy) and yawing moment distribution, integrated from the bow to the stern, for different grids

5 COMPARISON BETWEEN TOOLS AND DISCUSSION OF RESULTS

This section provides a comparative analysis of the numerical tools and examines the key findings of the study, with a specific focus on their dependency on water depth and closeness to the bank.

Ship forces and moments are expressed in the yawed-only coordinate system, which is nearly ship-fixed but remains level, excluding roll and pitch. This ensures the longitudinal and transverse axes stay in the earth-fixed horizontal plane. The origin is at the midsection centerline of the waterline intersection, with x-, y-, and z-axes directed forward, portside, and upward, respectively. The ship sway force and yaw moment are given in a non-dimensional form, using the ship speed V_s, water density ρ and draught at rest T. CFD calculations were performed at model scale, whereas RAPID and Flow Interaction code in XMF simulations were conducted at full scale. These non-dimensional loads are defined as follows:

$$F'_Y = \frac{F_Y}{0.5\ \rho\ L_{PP}\ T\ {V_S}^2} \qquad M'_Z = \frac{M_Z}{0.5\ \rho\ {L_{PP}}^2\ T\ {V_S}^2} \tag{1}$$

With F_Y and M_Z being the sway force and yaw moment respectively. The influence of confinement on surge force, having minimal impact, will be explored further in future studies.

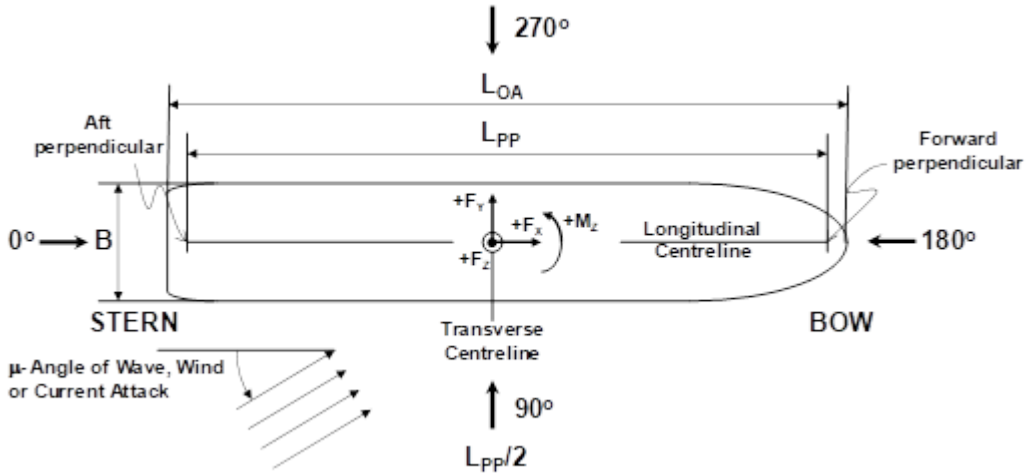

In all conditions, the ship experiences a transversal suction force (positive F_Y) directed towards the vertical bank, with the point of application located aft of midship, as indicated by the bow-out yaw moment (negative M_Z). The intensity of the bank effect increases as the under-keel clearance decreases. General observations from the tests show that forces tend to increase with higher speeds and closer proximity to the bank. The variation in the h/T plot indicates that at h/T = 3.0, there is strong agreement between the model test results, CFD simulations, and Flow Interaction calculations. Furthermore, the CFD results demonstrate improved alignment with model test data in shallow water conditions (h/T = 1.5 & 1.2), marking a significant step forward in using CFD as a reliable comparative tool for ship hydrodynamic analysis. However, the Flow Interaction results showed that the lateral force (F_Y) was approximately half the value measured in the basin, and the calculated moment was nearly negligible compared to the basin measurements. This suggests that the moment is significantly underestimated in both h/T = 1.5 and 1.2.

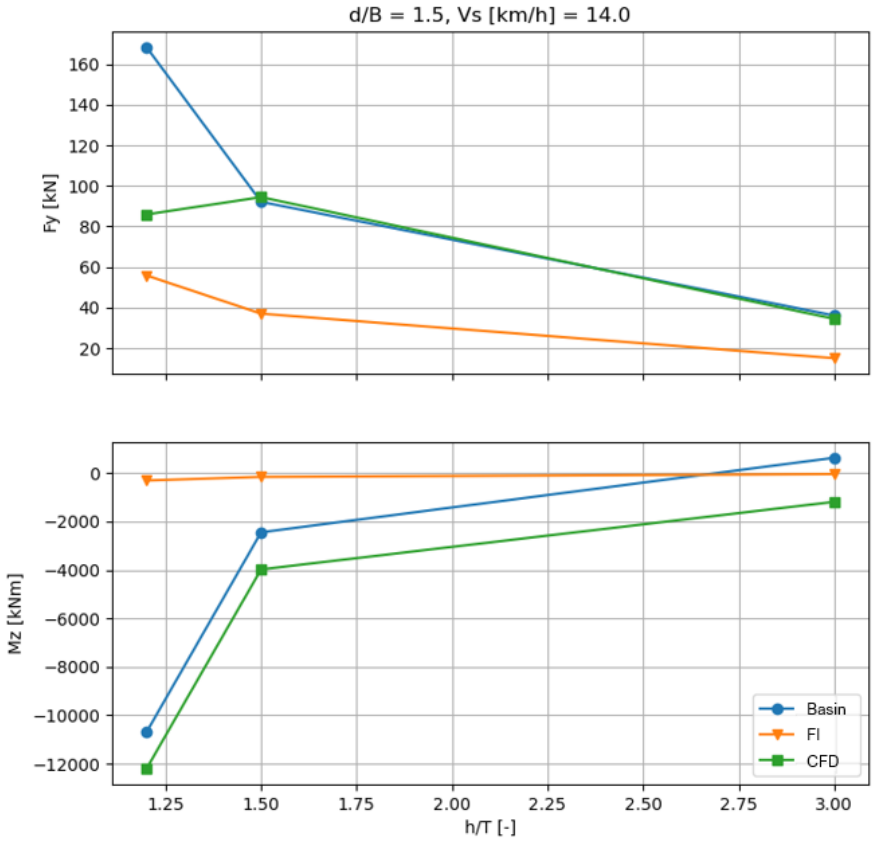

Figure 5. Suction force/moment trends in h/T in d/B=1.5 and speed 14 km/h.

Based on the findings, the focus is directed toward enhancing the Flow Interaction code by including alternative potential flow solvers like RAPID and systematically cross-referencing discrepancies between them. This approach aims to identify critical areas requiring refinement, ultimately improving the accuracy and reliability of the computational framework.

RAPID is one of the flow interaction codes that could provide valuable solutions for our analysis. It solves the exact fully non-linear potential flow problem by an iterative procedure, based on raised panel method (Raven, 1995, 1996 and 1998). The inviscid flow method neglects boundary layers and flow separation, overestimating stern waves, especially for fuller hulls. While wave resistance predictions are not fully accurate, the method is useful for hull design ranking. Wave breaking and spray are not modeled. RAPID has been extensively validated against MARIN's model test results, accurately predicting flow and wave patterns. It outperforms linearized methods in bow wave height and diverging wave predictions. While absolute wave resistance may vary, it is effective for comparing hull designs in optimization.

5.1 VARYING WATER DEPTH

For the case of h/T = 3.0, as illustrated in Figure 6, the plots present a comparison between CFD, RAPID (with and without trim and sinkage considerations) and Flow Interaction calculations. In this case, the trim has a negligible impact on the RAPID results. Specifically, RAPID demonstrates closer alignment with CFD results at both the bow and stern of the vessel, while Flow Interaction provides a marginally better match at midship. At the stern, both RAPID and Flow Interaction, as potential flow solvers, fail to accurately predict the increase in lateral force F_Y', which is primarily driven by viscous effects that are not captured by potential flow theory. These discrepancies highlight the limitations of potential flow methods in regions where viscous effects become significant.

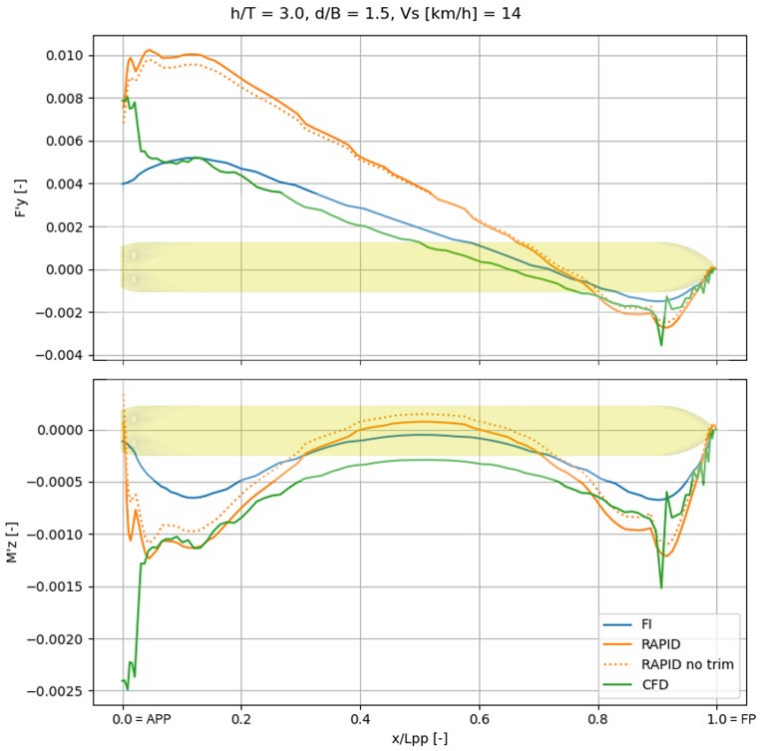

Figure 6: Case 02010401. Comparison of the integrated F'y and M'z.

This limitation becomes more evident when examining the pressure distribution comparison shown in Figure 7. In this comparison, the Flow Interaction results indicate an unrealistic pressure recovery near the stern, a characteristic that is typical of potential flow methods due to their inability to model viscous effects. This unrealistic recovery further underscores the challenge of accurately capturing flow behavior in the stern region using inviscid flow models.

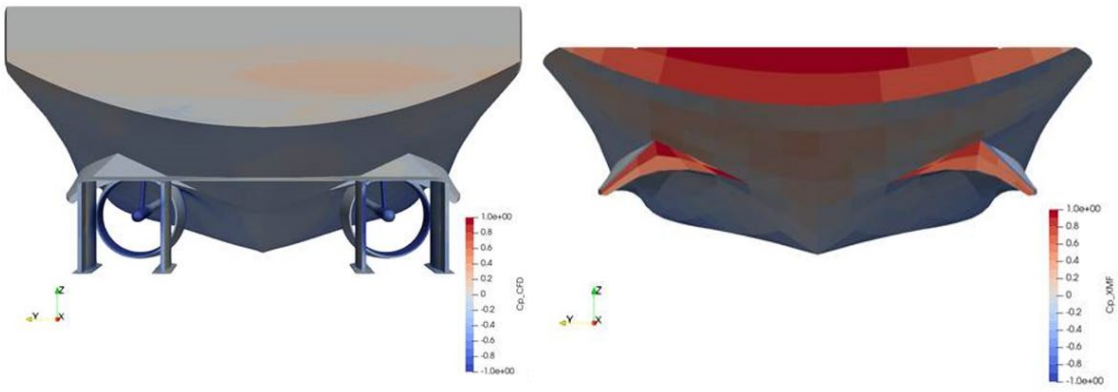

Figure 7. Case 02020401. Stern body. CFD results (left) and Flow Interaction calculations (right)

At the reduced water depth (h/T=1.5, see Figure 8), the Flow Interaction results exhibit a significant discrepancy with the CFD data, particularly at the bow. In contrast, RAPID more closely follows the CFD trend, effectively capturing the peak near the bow. Omitting trim and squat effects in RAPID improves the prediction of the lateral force (F_Y') compared to CFD; however, the deviations in the yaw moment (M_Z') are amplified. The primary distinction between RAPID and Flow Interaction lies in RAPID's incorporation of the free surface effects in its calculations, which could account for the observed differences between the two codes.

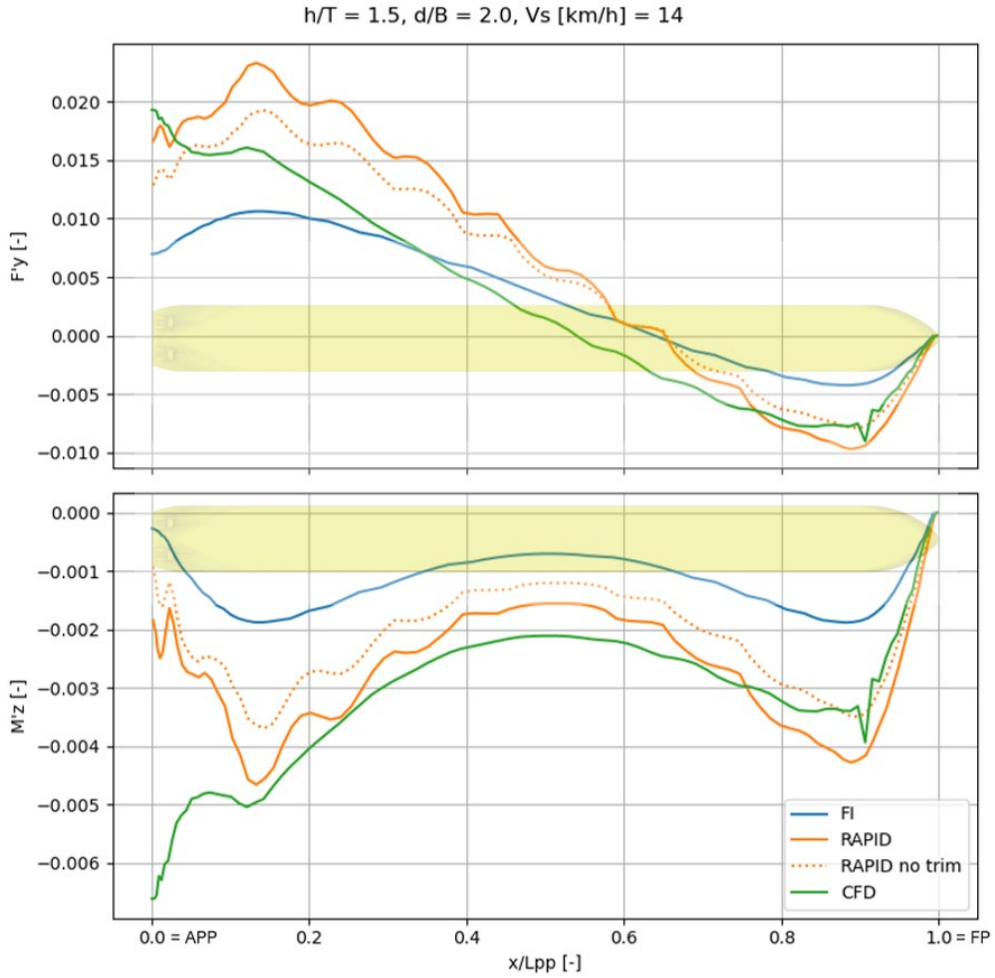

Figure 8. Case 03010201. Comparison of the integrated F'y and M'z.

At a water depth ratio of 1.2, the cumulative distributions for the lateral force F_Y' and yaw moment M_Z' coefficients, shown in Figure 9, reveal that RAPID aligns better with the CFD results. However, neither potential flow code accurately predicts the distribution at this shallow depth. This discrepancy is likely due to the increased significance of viscous effects, which are not captured by the potential flow models.

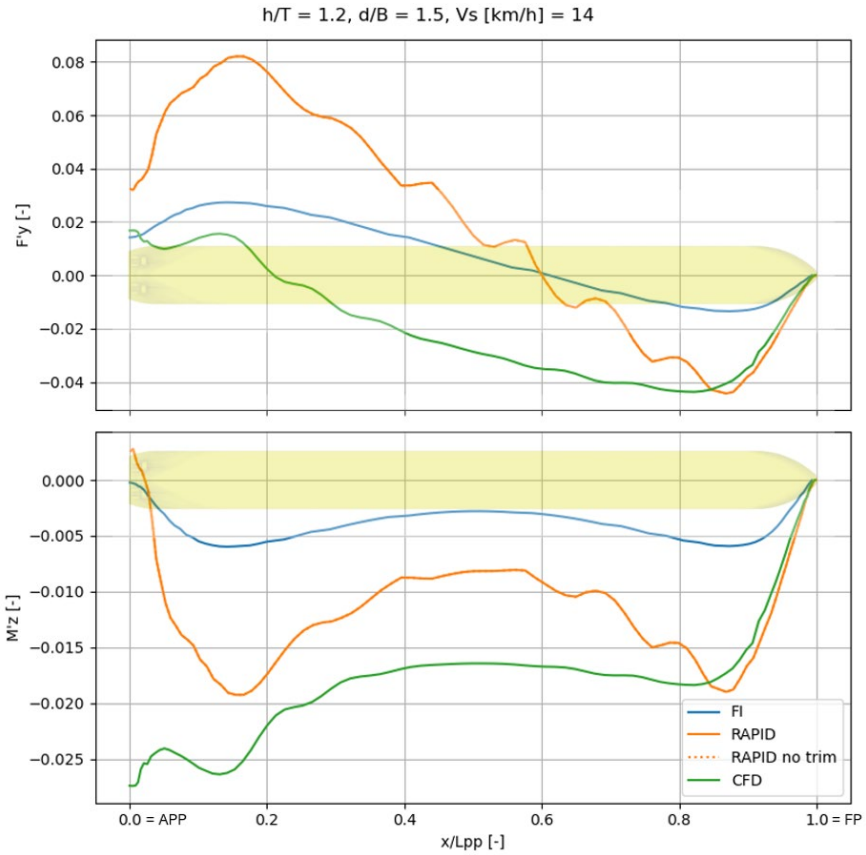

Figure 9. Case 04010401. Comparison of the integrated F'y and M'z.

A comparison between h/T = 1.2 (Figure 9) and h/T = 1.5 (middle plot in Figure 11) revealed that the M'_Z values at the bow are approximately three times greater in h/T = 1.2 in both CFD and RAPID results, see Figure 10.

For h/T = 1.5, the CFD maintains a smooth decline, while the RAPID shows pronounced fluctuations. Similarly, for h/T = 1.2, the CFD has a consistent trend, whereas the RAPID displays noticeable peaks and troughs. Overall, the CFD method is more stable and reliable for smooth trends, while the RAPID captures detailed changes, making it useful for applications requiring high sensitivity.

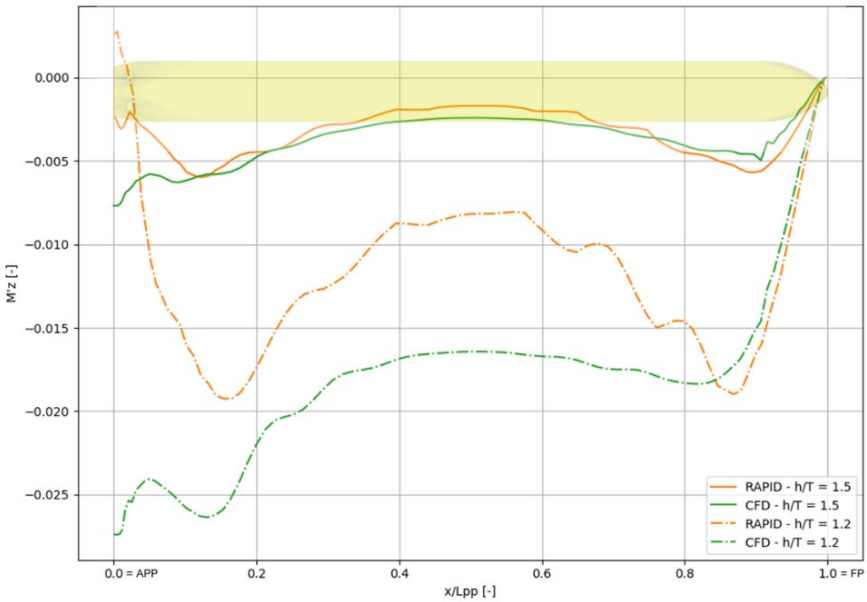

Figure 10. Comparison of the integrated M'z for h/T = 1.5 and h/T = 1.2

Figure 11 displays the dynamic pressure coefficient along the bow and stern at h/T=1.2. The high and low-pressure regions are consistent across all water depths, with increasing intensity as under-keel clearance decreases. At h/T = 1.2, the pronounced low-pressure zone beneath the hull indicates accelerated flow under the keel. Moreover, the pressure distribution exhibits greater asymmetry between the port and starboard sides, especially at the bow.

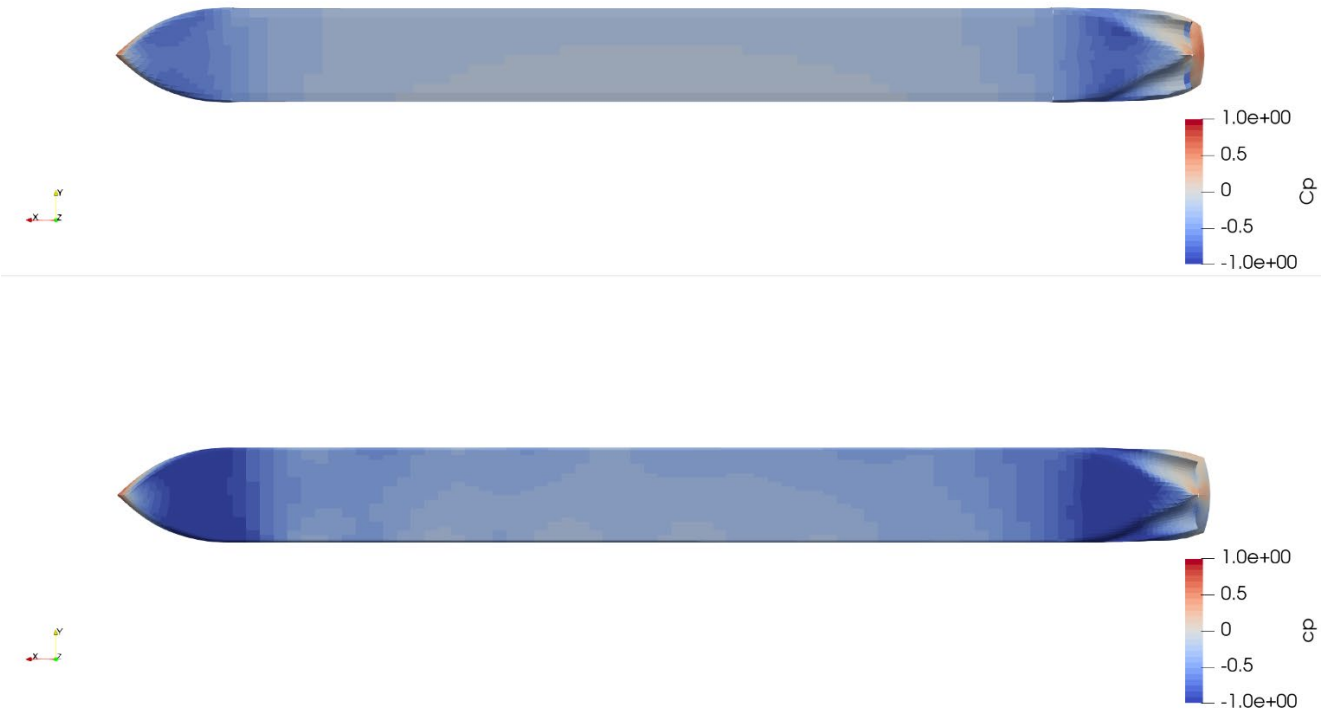

Figure 11. Dynamic pressure coefficient on the appended ship at Flow Interaction (top) and RAPID (bottom)

The differences between the Flow interaction code and RAPID can have different origins. The two more probable are free surface effects and dynamic trim and sinkage. Both of these phenomena are not taken into account in the Flow Interaction code. A small CFD study was conducted to estimate the importance of those effects on the side force. Figure 12 and Figure 13 show a comparison of between three cases: FreeSurf (with both free surface effect and dynamic trim and sinkage), Double body trim&sink (no waves but with dynamic trim and sinkage) and DoubleBody (no waves, no dynamic trim and sinkage). If we consider the free surface computations as the most accurate, then it seems that taking into account only dynamic trim and sinkage improves results, but it does not solve all of the issues. Hence, considering both seem to be required to predict ship bank interactions accurately.

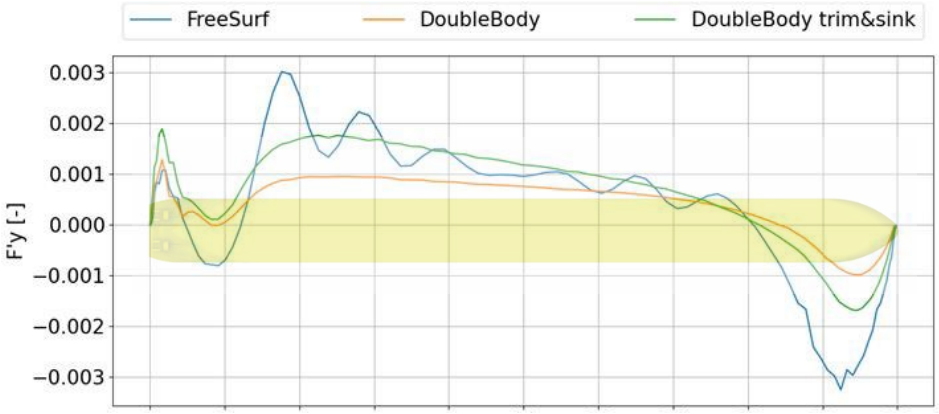

Figure 12. Longitudinal distribution of side force along the ship.

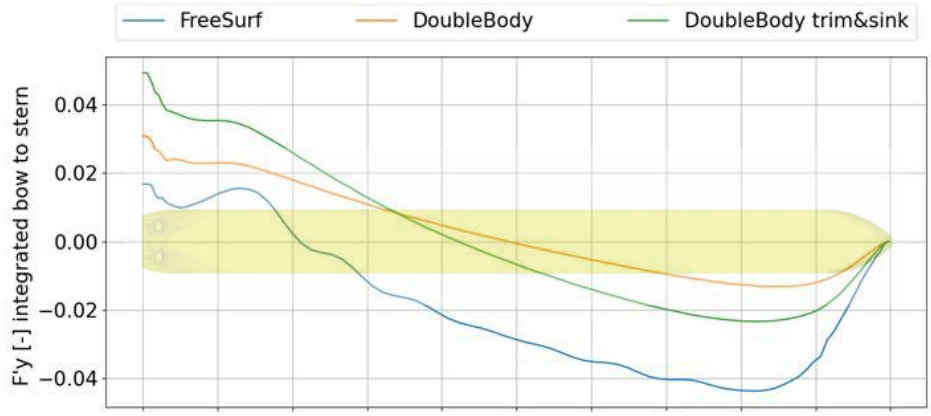

Figure 13. Longitudinal distribution of side force along the ship integrated from the bow to stern.

5.2 VARYING DISTANCE TO THE BANK

Figure 14 presents the integrated loads for various distances to the bank (2.0, 1.5, and 1.0 d/B). As the vessel approaches the bank, both F'_Y and M'_Z exhibit an increase. The differences between the results for 2.0 and 1.5 d/B are minimal. However, when reducing the distance to 1.0 d/B, a significant increase in forces is observed at the bow. This is attributed to the restricted flow of water between the vessel and the bank, resulting in enhanced interaction effects.

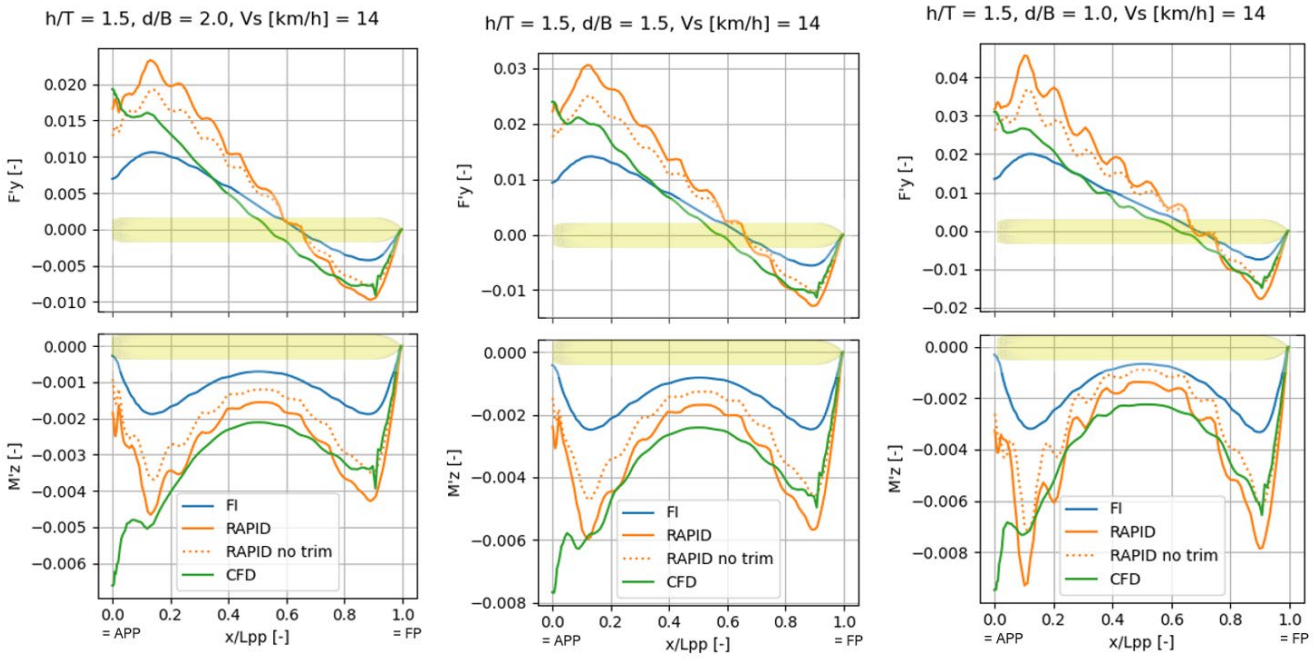

Figure 14. Comparison of the integrated F'y and M'z for h/T=1.5 at d/B=2.0 (left), 1.5 (middle) and 1.0 (right)

Based on the comparisons, it can be concluded that the influence of the h/T ratio (ranging from 1.5 to 1.2) has a more significant impact on the results than the effect of bank proximity at 1.5B. Furthermore, the distance to the nearest bank is sufficiently large to minimize any substantial viscous effects resulting from bank-induced interactions.

6 CONCLUSIONS

This research examines ship-bank interactions for a 135 m inland vessel in shallow water, using experimental and numerical methods under consistent conditions. The ship sails near a vertical bank in a shallow channel with a rectangular cross-section. The total width of the channel is 22.1B. The distance towards the closest bank varies between 2.0 to 1.0 B, therefore the system can be considered confined. Tests were conducted in a semi-captive setup with imposed surge, sway, roll, and yaw, while heave and pitch remained free. The analysis covers various bank distances (d/B) and water depths (h/T) at a speed of 14 km/h full scale. Experiments were performed under self-propulsion and water milling conditions for CFD validation, at three water depths (h/T = 3.0, 1.5, 1.2), four bank distances (d/B = 2.5, 2.0, 1.5, 1.0), and four speeds (8, 10, 12, 14 km/h).

Results show a transversal suction force (F_Y) toward the bank, with its point of application aft of midship, as indicated by the bow-out yaw moment (M_Z). The bank effect intensifies with reduced under-keel clearance, increased speed, and shorter bank distance. At h/T = 3.0 CFD, RAPID and Flow Interaction results align well. In shallower waters (h/T = 1.5 and 1.2), CFD more accurately predicts forces, while Flow Interaction code underestimates F_Y by approximately 50% and fails to capture M_Z. This suggests limitations in Flow Interaction XMF's modeling of bank-induced forces at low h/T. These findings support refining XMF simulations for improved hydrodynamic modeling in restricted waters.

The key findings from the study are as follows:

- **Deep Water Conditions (h/T > 3):** The Flow interaction code model performs reliably in deeper waters, showing reasonable agreement with CFD and RAPID simulations. The lower impact of viscosity in these conditions allows for accurate predictions. However, discrepancies arise near the stern, where Flow Interaction (as well as RAPID) fails to capture flow separation and other viscous effects, leading to deviations in the computed forces.
- **Moderate to Transitional Water Depths (1.2 < h/T < 1.5):** In moderately shallow waters, FI does not accurately predict the peak loads at the bow, resulting in significant differences from CFD results. RAPID, which accounts for free surface effects, provides a more accurate representation of these forces. This indicates that incorporating free surface modeling into FI could improve its predictive capability in transitional water depths.
- **Shallow Water Conditions (h/T= 1.2):** At very shallow depths, discrepancies between Flow Interaction, RAPID and CFD become more pronounced due to the increased influence of viscous effects such as turbulence and flow separation. The inability of the potential flow codes to account for these factors makes them unsuitable for precise force predictions in shallow water, highlighting the necessity for more advanced modeling techniques in these conditions.
- A CFD study demonstrated that while considering dynamic trim and sinkage improves results, it does not fully resolve all issues. Therefore, to accurately predict ship-bank interactions, both free surface effects and dynamic trim and sinkage must be taken into account.

The next phase of research will focus on evaluating the influence of trim, sinkage, and free surface effects—factors that are incorporated in RAPID but currently absent in Flow Interaction code in XMF. The primary objective is to enhance the Flow Interaction code in XMF's capability to accurately model ship-bank interactions in shallow water conditions (h/T = 1.5) by integrating these effects into the computational framework. It was confirmed by the CFD study that these effects have an important impact on hydrodynamic loads on the ship sailing along the regular bank.

To achieve this, a new computational module is planned for implementation. Once integrated, all test cases will be re-run to assess its impact on simulation accuracy and overall model performance. Additionally, an alternative approach under consideration involves developing an empirical correction node to account for the missing hydrodynamic effects, providing an adaptive solution to improve accuracy in shallow water conditions.

These enhancements will improve Flow Interaction code predictive accuracy, enabling more reliable simulations of ship-bank interactions across different water depths, particularly for typical cases encountered in real-time simulators.

7 REFERENCES

Bedos, A., Oud, G., De Boer, W., 2019. Impact of an Irregular Bank on the Sailed Trajectory of an Inland Ship. In: Proceedings of the Smart Rivers 2019 Conference. Lyon, France.

Bedos, A. Tonelli, R. Gornicz, T., 2025. Combining Numerical and Experimental Methods to Explain Ship Bank Interactions. MASHCON7.

Chillcce, G., Zentari, L., Van Hoydonck, W., Bedos, A., Ley, J., Gornicz, T., Yang, Y., Oud, G., Tenzer, M., Rzeszutko, J., el Moctar, O., 2025. Numerical Calculation of Hydrodynamic Forces on Inland Waterway Vessels During Circular Motion in Shallow and Extreme Shallow Waters. Ocean Engineering. Vol. 318. https://doi.org/10.1016/j.oceaneng.2024.120095.

Delefortrie, G., Verwilligen, J., Eloot, K., Lataire, E., 2024. Bank Interaction Effects on Ships in 6 DOF. Ocean Engineering. Vol. 310, Part 1. https://doi.org/10.1016/j.oceaneng.2024.118614.

Hess, J.L., Smith A. M. O. 1964. Calculation of Non-lifting Potential Flow about Arbitrary Three Dimensional Bodies. Journal of Ship Research, 6.

Korsmeyer, F. T, Lee C. H., Newman, J. N, 1993. Computation of Ship interaction forces in Restricted Waters. Journal of Ship Research. Vol. 37. No 4, pp 298-306.

Mai, T.L., Jeon, M., Vo, A.K., Yoon, H.K., 2023. A Numerical Study on the Ship–Bank Interaction at Various Water Depths of a Surface Ship. Science Progress. Vol. 106(1). https://doi.org/10.1177/00368504221149624.

Mucha, P., el Moctar, O., Dettmann, T., Tenzer, M., 2017. Inland Waterway Ship Testcase for Resistance and Propulsion Prediction in Shallow Water. Ship Technology Research. Vol. 64 (2), pp.106-113. https://doi.org/10.1080/09377255.2017.1349723.

Mucha, P., el Moctar, O., Dettmann, T., Tenzer, M., 2018. An Experimental Study on the Effect of Confined Water on Resistance and Propulsion of an Inland Waterway Ship. Ocean Engineering. Vol. 167, pp.11-22. https://doi.org/10.1016/j.oceaneng.2018.08.009.

Mucha, P., Dettmann, T., Ferrari, V., el Moctar, O., 2019. Experimental Investigation of Free-Running Ship Manoeuvres Under Extreme Shallow Water Conditions. Applied Ocean Research. Vol. 83, pp.155-162. https://doi.org/10.1016/j.apor.2018.09.008.

Newman, J. N. 1977. Marine Hydrodynamics. MIT. Press Cambridge.

Norrbin, N., 1985. Bank Clearance and Optimal Section Shape for Ship Canals. In: Proceedings of the 26th PIANC International Navigation Congress. Brussels, Belgium, pp. 167-178.

Raven, H. C., Valkhof, H. H. 1995 Application of Non-linear Ship Wave Calculations in Design. 6th PRADS Symposium, Seoul.

Raven, H. C.. 1996. A Solution Method for the Non-Linear Ship Wave Resistance Problem. PhD. Thesis, Delft University Technology.

Raven, H. C.. 1998. Inviscid Calculations of Ship Wavemaking Capabilities Limitations and Propect. 22nd Symposium on Naval Hydrodynamics. Washington DC.

Van Hoydonck, W., Toxopeus, S., Eloot, K., Bhawsinka, K., Queutey, P., Visonneau, M., 2019. Bank effects for KVLCC2. Journal of Marine Science and Technology. Vol. 24, pp. 174-199. https://doi.org/10.1007/s00773-018-0545-3.

Verwilligen, J., Lataire, E., Tello Ruiz, M., Eloot, K., 2022. Evaluation of Bank Effects on a Bulk Carrier in a Confined Channel Cased on Towing Tank Tests and Full-Scale Measurement. In: Proceedings of the 6th International Conference on Ship Manoeuvring in Shallow and Confined Water: Port Manoeuvres (MASHCON). Glasgow, UK, pp.285-298.

8 AUTHORS BIOGRAPHY

Marta Ibarrondo holds the position of Senior Project Manager at the Maritime Research Institute Netherlands (MARIN). She specializes in real-time simulators, modeling complex maritime and offshore operations for feasibility studies and crew training. She has conducted numerical research on shallow-water and maneuvering applications and advises Young NL PIANC's Maritime Navigation Commission on port and navigation guidelines.

Tomasz Gornicz holds the position of CFD Specialist at the Maritime Research Institute Netherlands (MARIN). He graduated from a technical university in Poland, where his professor, Jan Kulczyk, introduced him to the fascinating world of inland shipping hydrodynamics. For more than 10 years, he has been conducting numerical studies in ship manoeuvring and non-conventional propulsion systems.

Wim Kleermaker holds the position of Project Engineer within the Offshore department at the Maritime Research Institute Netherlands (MARIN). In this role, his main focus is on modelling all kinds of complex offshore systems in MARINs time domain software XMF.